Supporting Information

Movement to the clinic of soluble epoxide hydrolase inhibitor EC5026 as an analgesic for neuropathic pain and for use as a non-addictive opioid alternative

*Bruce D. Hammock,[§] Cindy B. McReynolds,[§] Karen Wagner,[§] Alan Buckpitt,[§] Irene Cortes-Puch,[§] Glenn Croston,[§] Kin Sing Stephen Lee,[#] Jun Yang,[§] William K. Schmidt,[§] Sung Hee Hwang[§,]**

[§]EicOsis Human Health Inc., Subsidiary of EicOsis LLC, 1930 5th Street, Suite A, Davis, CA 95616;
[#]Synthia LLC, P.O. Box 1238, Gualala, CA 95445

TABLE OF CONTENTS

LogP Measurement

LogP was determined using an Agilent HPLC 1200 series equipped with G1314 UV-vis detector and Phenomenex Luna reverse phase column (C18, 4.6 mm x 150 mm, 5 μm particle size) as previously published.[1] Briefly inhibitors (100 μM, 10 μL) were injected and run at isocratic gradient (MeOH:H_2O/ 2:1 (v:v)) for 90 min. The compounds were monitored at 230 nm. A calibration curve was generated using several compounds with LogP obtained from shake flask method and the retention time obtained from HPLC method. LogP values were calculated based on the calibration curve.

Solubility determination

Each inhibitor (1mg) was suspended in the phosphate buffer (0.1 M Sodium Phosphate, pH 7.4, 300 μL). The suspension was shaken (220 rpm) at rt for 24h. The suspensions were centrifuged at 10,000 rpm for 10 min at rt (Centrifuge 5415D, Eppendorf, Hauppauge, NY). The supernatant was transferred to a 1.5 mL eppendorf tube and was further diluted 10 times by MeOH. The solution was kept on ice for 15 min to precipitate the salt. The solution was centrifuged at 10,000 rpm for 10 min at 4 ℃ (Accuspin™ MicroR, thermo Fisher, Freemont, CA) and the supernatant was transferred to 1.5 mL vial and was kept at -20℃ before LC-MS/MS analysis.

FRET-Displacement assay procedure

The FRET assay was performed as published previously.[121,2] sEH inhibitor stock solution (10 mM, DMSO) was stored in glass vials. Recombinant sEH was diluted to the desired concentration (20 nM) with phosphate buffer (100 mM sodium phosphate, pH 7.4, 0.01% gelatin. All buffer used in this assay was filtered with a sterilized filtration unit (Millipore® Durapore PVDF Membrane, pore size: 0.22 μm)

Measurement in 96-well plates: All the measurement for FRET- based displacement assay in 96-well plate format was done in TECAN Infinite® M1000 Pro.

Pre-treatment of 96-well plate: 96-Well plates were pre-incubated with PB with 0.01% gelatin overnight at rt. The gelatin coats the plate and prevents the loss of sEH and sEH inhibitors to the plate via non-specific binding. The buffer was then discarded, and the plate was dried before use.

K_i Assay procedure: The sEH stock solution was diluted to the desired concentration (20 nM) by PBS (100 mM sodium phosphate, 0.1 % gelatin, pH 7.4). ACPU (one equivalent to sEH, 10 mM, Ethanol) was added to the sEH solution and was incubated for 2h at rt. The sEH-ACPU mixture (20 nM, 100 mM sodium phosphate, 0.1 % gelatin, pH 7.4, 150 μL) was added to each well. The baseline fluorescence (F_0) (λ_{ex} at 280 nm, λ_{em} at 450 nm) of the samples was measured after the z-position and gain were optimized automatically by the fluorometers. The z and gain

value were noted and will be used for the later fluorescent measurement. Because DMSO has been known to quench fluorescence. 1% DMSO in PB was served as a control (F_{DMSO}). The desired concentration of inhibitors which is the concentration that 100% of sEH was bound to inhibitor, was added at the first well and was further diluted by 2-fold across the rest of the wells. Based on our study, 12 datum points which correspond to 12 different concentrations of the inhibitor, generated sufficient data to calculate the accurate K_i for the inhibitors. The samples were incubated at 30 ˚C for 1.5h. Then, the fluorescence (λ_{ex} at 280 nm, λ_{em} at 450 nm) of the samples was measured using the z-position and gain values that previously obtained. The obtained fluorescence signals were transformed as below and were used to calculate the K_i of the inhibitors according to "Curve fitting" section below.

Initiated fluorescence = $F_{DMSO\ (well\ X)} / F_{0\ (well\ X)}$
Saturated fluorescence = $F_{at\ the\ saturated\ concentration\ (well\ X)} / F_{0\ (at\ well\ X)}$
Observed fluorescence = $F_{(well\ X)} / F_{0\ (well\ X)}$

Curve fitting: Curve fitting for K_i determination was reported before.[2] The data manipulation and K_i calculation were based on previous publications.[3,4]

The displacement assay is based on a three-state equilibrium binding model. This is modeled as described below (Eq. 1)

$$[RI] + L \leftrightarrow R + I + L \leftrightarrow [RL] + I \qquad \text{(Eq. 1)}$$

where [RI] = receptor or enzyme-inhibitor complex; L = reporting ligand; I = inhibitors;
[RL] = receptor or enzyme-reporting ligand complex.

The three-state equilibrium (Eq. 1) consists of the sEH-inhibitor complex, sEH and sEH-reporting ligand complex. In this study, the relative fluorescence intensity (F_3) was plotted against the concentration of sEH inhibitor and the resulting curve was fitted into equation (Eq. 2) derived by Wang *et al.* for three-state equilibrium.[9]

$$F_3 = \left[2(a^2 - 3b)^{1/2}\cos(\theta/3) - a\right] / \left\{3K_{d1} + \left[2(a^2 - 3b)^{1/2}\cos(\theta/3) - a\right]\right. \qquad \text{(Eq. 2)}$$

with $a = K_{d1} + K_{d2} + L + I - R$;
$b = K_{d2}(L - R) + K_{d1}(I - R) + K_{d1}K_{d2}$;
$c = -K_{d1}K_{d2}R$; and
$\theta = \arccos\left\{(-2a^3 + 9ab - 27c) / \left[2(a^{2-3b})^{3/2}\right]\right\}$.

where F_3 = Relative Fluorescence = (observed fluorescence – fluorescence at saturation)/ (initiated fluorescence – fluorescence at saturation); I = the concentration of added unlabeled competing ligand; R = the total concentration of sEH; L = The total concentration of reporting ligand; K_{d1} = The dissociation constant of reporting ligand (found by fluorescent binding assay); and K_{d2} = The inhibition constant of inhibitors

k_{off} (t_R) measurement procedure: k_{off} Measurement was run as described before.[1,3] sEH (8 μM) was pre-incubated with the selected inhibitor (8.8 μM, 100 mM PB buffer, pH 7.4) for 1.5 h at rt. The sEH-inhibitor complex was then diluted 40 times with ACPU (20 μM, 100 mM Sodium phosphate buffer, pH 7.4). The fluorescence (λ_{ex} at 280 nm, λ_{em} at 450 nm) was monitored immediately for every 30s up to 5100s. The fluorescence (λ_{em} at 450 nm) data was plotted against time (s). The resulting curve was fitted to single exponential growth and the relative k_{off} was obtained. t_R is $1/k_{off}$.

PK analysis

Male SD rats were used in PK studies. Selected inhibitors were dissolved in 100% PEG 300 to give a clear solution and 100 μL of the inhibitor solution (0.1 mg/kg) was administered to the rats via oral gavage. The blood samples (10 μL) were then collected from tail vein using pipet tip pre-washed with 7.5% EDTA(K_3) at time 0, 0.5, 1, 2, 4, 6, 8, 24 and 48 h after administration of the inhibitors. The collected blood samples were immediately transferred to an Eppendorf tube (1.5 mL) containing 50 μL of 0.1% EDTA (by weight) solution and mixed strongly. The samples were stored at -80 ˚C until analysis. The blood samples were then prepared based on the published procedure for LC-MS/MS analysis.[1] PK parameters of individual mice were calculated by fitting the time course curve of blood concentration data to a one-compartmental analysis with the WinNonlin software (Pharsight, Mountain View, CA). Parameters calculated include time of maximum concentration (T_{max}), maximum concentration (C_{max}), half life ($t_{1/2}$), and area under the concentration–time curve to terminal time (AUC_t). AUC was calculated by the linear/log trapezoidal rule.

Table S1. Equilibrium Solubility of EC5026 in Aqueous and Non-Aqueous Systems

Solvent	Equilibrium Solubility (mg/mL)
Deionized water	< 0.1
pH 1 Hydrochloric acid	< 0.1
pH 7.4 Phosphate buffer	< 0.1
pH 10 Sodium hydroxide	< 0.1
50% PEG 300/50% water	0.4
PEG 300	13.9
PEG 400	14.0
FaSSIF	< 0.1
FeSSIF	0.2
Glycerol	< 0.1
Propylene glycol	24.1
Tween 80 @ 1, 5, 10 and 100 x CMC (CMC = 12 μM)	< 0.1
Sodium lauryl sulfate 8.2 mM (1 x CMC)	0.03
Sodium lauryl sulfate 41.0 mM (5 x CMC)	1.2
Sodium lauryl sulfate 82.0 mM (10 x CMC)	1.5
Sodium lauryl sulfate 8.2 M (100 x CMC)	2.5
TPGS	40.6[a]
50% Sulfobutylether β-CD 0	7.9
Castor oil	5.5
Castor oil, hydrogenated	42.6[a]
Soybean oil	< 0.1
Corn oil	< 0.1
Canola oil	< 0.1
Captex 355 EP, NF	2.0
Miglyol 810	2.0
Miglyol 812	1.9
Capmul MCM EP	24.5
Capmul MCM NF	56.2[a]
Kolliphor P188/water (1:1)	1.4
Kolliphor HS-15	37.3[a]
Kolliphor EL	20.4
Oleic acid	9.0
Plurol Oleique CC 497	8.7
Peceol	12.9
Labrasol	21.8
Labrafil M1944CS	9.6
Triacetin	6.4
Transcutol HP	38.1
Gelucire 44/14	37.7[a]
Intralipid®	0.1

Abbreviations: PEG = polyethylene glycol; CD = cyclodextrin; CMC = critical micelle concentration; FaSSIF = fasted state simulated intestinal fluid; FeSSIF = fed state simulated intestinal fluid; TPGS = *d*-α-tocopheryl polyethylene glycol 1000 succinate. [a]Heated to 75 ºC to melt

In Vitro Absorption of EC5026

P-gp Inhibition: An *in vitro* study with MDR1-MDCKII cells was contracted with Cerep (Redmond, WA) to assess permeability and potential P-gp inhibition by EC5026. EC5026 demonstrated high permeability that is partly mediated by P-gp transport and no intestinal secretion. Calcein AM, an excellent substrate of P-gp, was used as a probe substrate for the P-gp inhibition study. At 10 μM, EC5026 caused a small, less than 25% inhibition of the P-gp mediated transport of Calcein AM. These results suggest that EC5026 is not a potent P-gp inhibitor.

Table S2. In vitro permeability data of EC5026 using Caco-2 cells at 10 μM in DMSO

	Permeability (10-6 cm/s)			Percent Recovery (%)		
	1st	2nd	Mean	1st	2nd	Mean
A-B permeability (pH 7.4/7.4)	27.01	25.78	26.4	47	46	47
A-B permeability (pH 7.4/7.4 + verapamil)	19.09	14.38	16.7	46	40	43
B-A permeability (pH 7.4/7.4)	16.17	16.60	16.4	81	81	81
B-A permeability (pH 7.4/7.4 + verapamil)	22.48	23.48	23.0	99	82	90

[a]Conditions: the cells were incubated at 37 °C for 60 min and the concentrations of EC5026 were detected by LC-MS/MS

Permeability analysis:[5] The apparent permeability coefficient (P_{app}) of the test compound was calculated as follows:

$$P_{app}(cm/s) = \frac{V_R * C_{R,end}}{\Delta t} * \frac{1}{A*(C_{D,mid}-C_{R,mid})}$$

where V_R is the volume of the receiver chamber. $C_{R,end}$ is the concentration of EC5026 in the receiver chamber at the end time point, Δt is the incubation time and A is the surface area of the cell monolayer. $C_{D,mid}$ is the calculated mid-point concentration of the test compound in the donor side, which is the mean value of the donor concentration at time 0 minute and the donor concentration at the end time point. $C_{R,mid}$ is the mid-point concentration of EC5026 in the receiver side, which is one half of the receiver concentration at the end time point. Concentrations of EC5026 were expressed as peak areas of EC5026.

Recovery of the Test Compound from the Permeability Assay The recovery of EC5026 was calculated as follows:

$$Recovery(\%) = \frac{V_D * C_{D,end} + V_R * C_{R,end}}{V_D * C_{D0}} * 100$$

where V_D and V_R are the volumes of the donor and receiver chambers, respectively. $C_{D,end}$ is the concentration of EC5026 in the donor sample at the end time point. $C_{R,end}$ is the concentration of EC5026 in the receiver sample at the end time point. C_{D0} is the concentration of EC5026 in the donor sample at time zero. Concentrations of EC5026 are expressed as peak areas of EC5026.

Fluorescein assessment for permeability assay Fluorescein was used as the cell monolayer integrity marker. Fluorescein permeability assessment (in the A-B direction at pH 7.4 on both sides) was performed after the permeability assay for the test compound. The cell monolayer that had a fluorescein permeability of less than 1.5 x 10^{-6} cm/s for Caco-2 cells was considered intact, and the permeability result of EC5026 from intact cell monolayer is reported.

Description of Manufacturing Process of EC5026 and Placebo Capsules

EC5026 capsules were prepared in accordance with pharmacy compounding procedures at the clinical site pharmacy and the United States Pharmacopeia (USP) <795> Pharmaceutical Compounding – Nonsterile Preparations

The compounding process is performed as follows:

1. The compounding area was cleaned per checklist.
2. Analytical balances were calibrated per written procedure.
3. The number of capsules required for the batch being compounded was checked and finalized.
4. The compounding area was staged with the materials to prepare EC5026 or placebo capsules.
5. The average capsule weight was determined on 10 sets of 10 randomly selected empty capsules (100 capsules in total).
6. ProFiller® was set up, capsules were oriented, and caps were separated from the bottoms of the capsules.
7. The amounts of PEG 400, PEG 3350 and EC5026 (including a 30% overage) required to prepare the specified number of capsules for the batch were calculated.
8. An appropriately sized USP Type 1 glass-mixing vessel capable of holding the entire volume of the batch was selected and equipped with a suitable mixing device.
9. The calculated amount of PEG 400 from Step 7 was weighed into the mixing vessel.
10. The calculated amount of PEG 3350 from Step 7 was weighed into a weighing container and transferred to the mixing vessel.
11. The calculated amount of EC5026 from Step 7 was weighed and transferred to the mixing vessel.
12. The mixing vessel was placed onto a stirring plate equipped with a heating element.
13. The heating element was set to ~70 ºC and the mixing was started. The stirring speed was adjusted to ensure adequate mixing.
14. Mixing was continued at 70 ºC until a clear solution is obtained.
15. The bulk solution was maintained at ~70 ºC throughout the capsule filling process.
16. Filling of the capsules was performed using HandiStep® Electronic Repeating Pipette set to dispense 500 µL of the heated solution.
17. The capsules were filled by withdrawing the heated clear solution with the electronic pipette, wiping the tip of the pipette, dispensing and discarding the initial 500 µL of solution and then dispensing 500 µL into each capsule filling a maximum of 20 capsules before reloading the pipette.
18. Once 20 capsules were filled, dispense the remainder of the solution in the pipette to waste and refill the pipette. Note: The same pipette tip was used to fill the entire batch of capsules.
19. Step 17 was repeated until all capsules are filled.
20. Step 13 to 17 should be completed within 8 hours.
21. Filled capsules were allowed to cool to room temperature for a minimum of 45 minutes.
22. Once cooled, the capsules were closed with the caps and the gross weight of each individual capsule was determined.
23. The fill weight of each capsule was calculated by subtracting the average capsule weight (Step 4) from the gross weight of the capsule containing the solution and recorded.

24. If the fill weight of the capsule falls outside of the fill weight control limits as described in the Table below, it was rejected.

Table S3. Acceptance criteria for capsules.

Capsule Strength	Nominal Fill Volume	Nominal Fill Weight	Tolerance	Control Limits
0.5 mg	500 µL	545 mg	± 5%	518 mg – 572 mg
8 mg	500 µL	545 mg	± 5%	518 mg – 572 mg

25. Acceptable capsules were placed into the container closure system, which is sealed with a cap.
26. The container closure system was labeled with a preprinted label and stored at 15 - 30 ºC.

Experiments for CYP induction and CYP inhibition

CYP induction studies were conducted at Sekisui Xenotech, Kansas City, KS and assessed by RT-PCR analysis of CYP mRNA in cultured hepatocytes treated once daily for three days with EC5026 at concentrations of 0.3, 1, 3, 10, 30 or 100 µM. CYP1A2, 2B6 and 3A4 mRNA was evaluated 24 hours following 3-days of once daily treatment and compared to positive and negative controls.

Human hepatocytes were prepared from 3 individual donors, cryopreserved and characterized for CYP activity and viability prior to use in this study. Hepatocyte cultures were treated once daily for three consecutive days and cultured according to established standard operating procedures and previously described methods.[6] Cultures were treated with supplemented MCM (each culture well was treated with 0.2 ± 0.02 mL at approximately 37 °C) containing 0.1% v/v DMSO (vehicle control), flumazenil (25 µM, negative control), one of six concentrations of EC5026 (0.3, 1, 3, 10, 30 or 100 µM), or one of three known human CYP enzyme inducers, namely, omeprazole (50 µM), phenobarbital (750 µM) and rifampin (20 µM), positive controls. The culture multi-well plates were placed in a humidified culture chamber (37 ± 1 °C at 95% relative humidity, 95/5% air/CO2). Approximately 24 h following the final treatment, cultures were visualized with a Nikon TMS Microscope (Nikon Corporation) or Accu-Scope 3020 Inverted Microscope (Accu-Scope Inc.), and a representative well from each treatment group was photographed with a PAXcam5 (MIS Inc.) digital camera to document morphological integrity.

Approximately 24 h after the last treatment hepatocytes were lysed in Buffer RLT reagent containing β-mercaptoethanol (100:1), and cell lysates were stored at −80 ± 10 °C. For each human

hepatocyte preparation, media from three or six wells per treatment group were aspirated and approximately 250 µL Buffer RLT was added to each well. The cell lysates were mixed by shaking for 10 min at 800 rpm. Total RNA was isolated using the RNeasy Mini Kit (Qiagen Inc.). RNA quality and concentration were determined by measuring absorbance at 260 and 280 nm on a BioTek Synergy HT plate reader (BioTek Instruments, Inc.) with KC4 Signature software (version 3.4 rev 21, BioTek Instruments, Inc.) according to internal SOPs. Single-stranded cDNA was prepared from RNA with the RT Master Mix using the AB 7900HT Fast Real Time PCR System thermocycling program (Applied Biosystems). The RT Master Mix is comprised of 10X RT buffer, 25X deoxyNTPs, 10X Random hexamers, RNase Inhibitor (20 U/µL), MultiScribe reverse transcriptase (50 U/µL) and RNase-free water. The RT Master Mix was added to each RNA sample to complete the components of the reaction. No template controls (NTCs) were included in the analysis. For the NTC reactions, RNase-free water was added in place of the RNA sample. The prepared cDNA samples were stored at −20 ± 5 °C following analysis by qRT-PCR.

Quantitative RT-PCR was carried out according to standard operating procedures and the Applied Biosystems protocol. Each PCR was performed in triplicate. A Primer Mix was prepared for each Gene Expression assay. A typical Primer Mix contained TaqMan Fast Advanced Master Mix (1X), Gene Expression Assay (1X, 900 nM forward and reverse primers) and RNase-free water. The Reaction Mix was prepared by adding the Primer Mix to cDNA. A percentage of samples (no less than 10%) included NACs. NACs are RNA samples that are not reverse transcribed and are used to show that mRNA, not genomic DNA, is the source of PCR's fluorescent signal. Reactions were analyzed on an Applied Biosystems Real Time PCR sequence detection system (AB 7900HT). The relative quantity of the target cDNA compared with that of the control cDNA (GAPDH) was determined by the ΔΔCt method (Applied Biosystems User Bulletin #2). Relative quantification measures the change in mRNA expression in a test sample relative to that in a control sample (e.g., DMSO). This method assumes that the efficiency of the target amplification and the efficiency of the endogenous control amplification are approximately equal.

mRNA by qRT-PCR

For qRT-PCR, data were processed and graphed using a LIMS (includes Galileo version 3.3, Thermo Fisher Scientific Inc. and reporting tool, Crystal Reports 2008, SAP) and the Sequence Detection System (SDS) Software version 2.4, for Relative Quantification (Applied Biosystems).

This software analyzes relative gene expression using the comparative Ct method (ΔΔCt), which relates the PCR signal of the target transcript to the PCR signal of the target in an untreated control. Both the treated sample and the untreated control signals are normalized to the endogenous control (GAPDH), for which expression is not affected by treatment and expression is constant throughout the tissue being tested. The results of this method are expressed as a fold change in expression with respect to the target transcript expression in the untreated control.

Calculations are as follows:

1. ΔCt = Ct (target) − Ct (endogenous control)
2. ΔΔCt = ΔCt (treated sample) − ΔCt (untreated control)
3. Fold change in expression = 2−ΔΔCt

An algorithm within the software automatically removed outliers from analysis. The statistical method used by the software is based on a modified Grubbs outlier removal (also known as the Maximum Normalized Residual Test), which permits the exclusion of a single outlier in a population consisting of as few as three replicates. However, if an apparent outlier is within 0.25 Ct of the mean for the associated replicate group, the software does not remove it. Outliers are considered to be wells with Ct values that differ significantly from associated replicate wells and typically are wells that did not amplify sufficiently if at all.

The level of mRNA expression relative to the positive control was calculated as follows:

Percent positive control = [(Fold change in treated sample) – 1] [(Fold change in positive control) – 1] × 100

In addition, where fold change was < 1, percent decrease was calculated as follows:

Percent decrease (%) = [Fold change (vehicle control) – Fold change (test drug treated cells)] × 100

CYP inhibition studies were conducted at EicOsis, LLC (Davis, CA) and completed using isoform selective substrates in a validated 'cocktail' assay with human liver microsomes (Sekisui Xenotech, Kansas City, KS) as described by Otten, Hingorani, Hartley, Kragerud and Franklin[7] (2) and outlined in Tables 1 and 2.

Briefly, incubations were performed in 10 x 75 mm glass disposable culture tubes in a total volume of 100 µl. Substrate was added first in 1 µl solvent using a 10 µl glass syringe. This was followed by additions of 0.1 M sodium phosphate buffer, pH 7.4 or EC5026 dissolved in phosphate buffer (10 µM-near the limit of solubility yielding final concentrations of 7 µM). Freshly thawed

human liver microsomes (100 μg protein) were added and incubation vials were transferred to a shaking incubator at 37°C with 100 oscillations/min. After a 2 min preincubation period, NADPH was added to the tubes at 30 sec intervals to start the reaction. Following a 10 min incubation, 200 μl ice cold methanol containing the internal standard (labetalol 0.1 μM) was added to quench the reaction. Reaction contents were stored at -20 °C until analysis by LC/MS/MS.

To test the possibility that EC5026 could inhibit any of the CYP isoforms by formation of a metabolite inhibitor complex or by generation of a tight binding metabolite (suicide substrate), the experiments described above were repeated with the exception that EC 5026 was incubated with human liver microsomes in the presence of NADPH for 20 min prior to the addition of isoform selective substrate. No significant inhibition of the metabolism of any of the isoform selective substrates was noted in these studies (data not shown).

Table S4. Isoform selective substrates and inhibitors of human cytochrome P450 enzymes

P450	Substrate	Substrate conc μM (solvent)	Metabolite	MS/MS transition	Source
1A2	phenacetin	100 (methanol)	acetaminophen	152.2→110.1 (+)	Sigma
2B6	Buproprion	125 (methanol)	hydroxybupropion	256.2→139.1 (+)	Sigma
2C8	Amodiaquine	1 (water)	N-desethylA	328.1→283.0 (+)	Sigma
2C9	tolbutamide	100 (methanol)	hydroxytolbutamide	285.1 →186.0 (-)	Sigma
2C19	S-mephenytoin	50 (acetonitrile)	hydroxymephenytoin	235.1→133.1(+)	Cayman
2D6	dextromethorphan	2.5 (methanol)	dextrorphan	258.1 →157.1(+)	Sigma
3A4/5	midazolam	2.5 (methanol)	hydroxymidazolam	342.1 →324.0	Cerilliant
3A4/5	testosterone	50 (acetonitrile)	6β-OH testosterone	305.2 →269.2	Cerilliant

Labetalol (Sigma) was used as an internal standard and was detected in positive ionization mode using the 329→162 transition.

Table S5. Inhibitors used as positive controls in the CYP450 assays

P450	Inhibitor	Inhibitor Concentration (solvent)	Source
1A2	furafylline	4 μM (ethanol)	Cayman Chemical
2B6	ticlopidine	0.7 μM (methanol)	Sigma
2C8	Quercetin	6 μM (methanol)	Cayman
2C9	sulfaphenazole	0.5 μM (methanol)	Cayman
2C19	ticlopidine	3.5 μM	Sigma
2D6	quinidine	0.5 μM (methanol)	Sigma
3A4/5	ketoconazole	0.1 μM(methanol)	Cayman

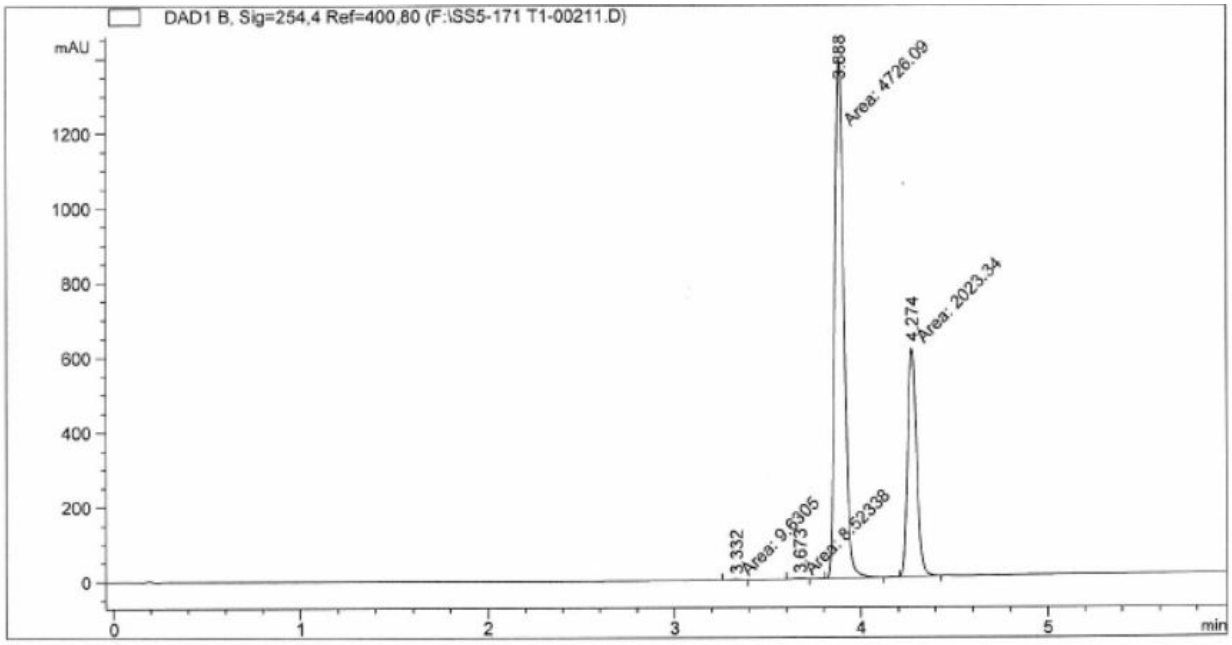

Area Percent Report

Sorted By : Signal
Multiplier : 1.0000
Dilution : 1.0000
Do not use Multiplier & Dilution Factor with ISTDs

Signal 1: DAD1 B, Sig=254,4 Ref=400,80

Peak #	RetTime [min]	Type	Width [min]	Area [mAU*s]	Height [mAU]	Area %
1	3.332	MM	0.0684	9.63050	2.34743	0.1423
2	3.673	MM	0.0607	8.52338	2.34020	0.1259
3	3.888	MM	0.0564	4726.08691	1397.62561	69.8342
4	4.274	MM	0.0546	2023.34302	617.06696	29.8976
Totals :				6767.58380	2019.38019	

Figure S1. In-process HPLC analysis of EC5026

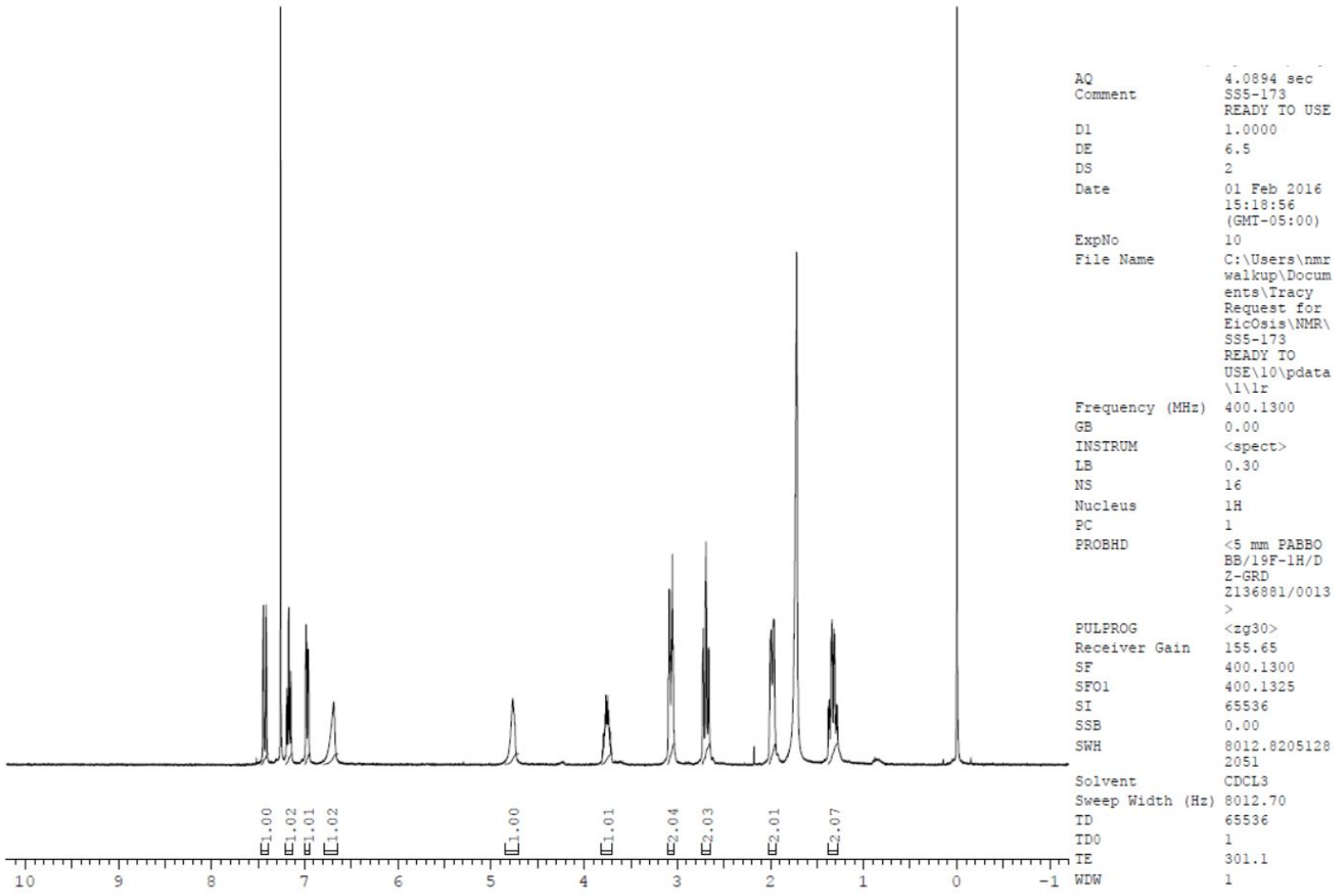

Figure S2. ^{1}H NMR of the compound **5**.

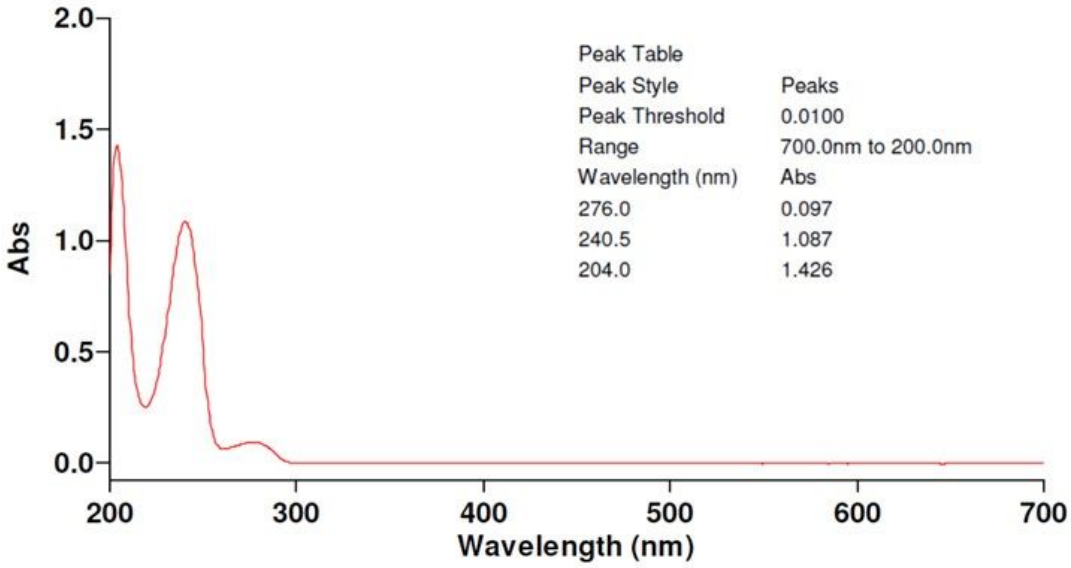

Instrument Parameters

Instrument	Cary 60
Instrument Version	2.00
Start (nm)	700.0
Stop (nm)	200.0
X Mode	Nanometers
Y Mode	Abs
UV-Vis Scan Rate (nm/min)	60.000
UV-Vis Data Interval (nm)	0.50
UV-Vis Ave. Time (sec)	0.5000
Beam Mode	Dual Beam
Baseline Correction	On
Baseline Type	Baseline correction
Baseline File Name	CARY60-PC\SQLEXPRESS|VAIMDB_Data(000)|Sample ss5176.BSW
Baseline Std Ref File Name	
Cycle Mode	Off
Comments	

The sample solution was prepared in MeOH at 0.0169 mg/mL.

Figure S3. UV-Vis spectrum of EC5026.

```
Acq. Operator   : System Administrator
Sample Operator : Analytical
Acq. Instrument : LCMS3                          Location :   34
Injection Date  : 2/9/2016 5:28:32 PM
                                                 Inj Volume : 2.000 µl
Acq. Method     : C:\Chem32\1\Methods\Sa50Pos.M
Last changed    : 11/5/2015 7:51:44 AM by sysadmin
Analysis Method : C:\Chem32\1\Methods\Sa50PosRpt.M
Last changed    : 10/26/2015 7:11:16 AM by sysadmin
                  (modified after loading)
Method Info     : SorbTech C18AQ, 2.1 x 50 mm, 3 um
                  Gradient method: 5-95% ACN + 0.1% Formic acid in Water + 0.1% Formic acid
                  in 14 min, hold at 95% ACN + 0.1% Formic acid for 4 min

Sample Info     : Walkup method: 'SA50Pos'

Additional Info : Peak(s) manually integrated
```

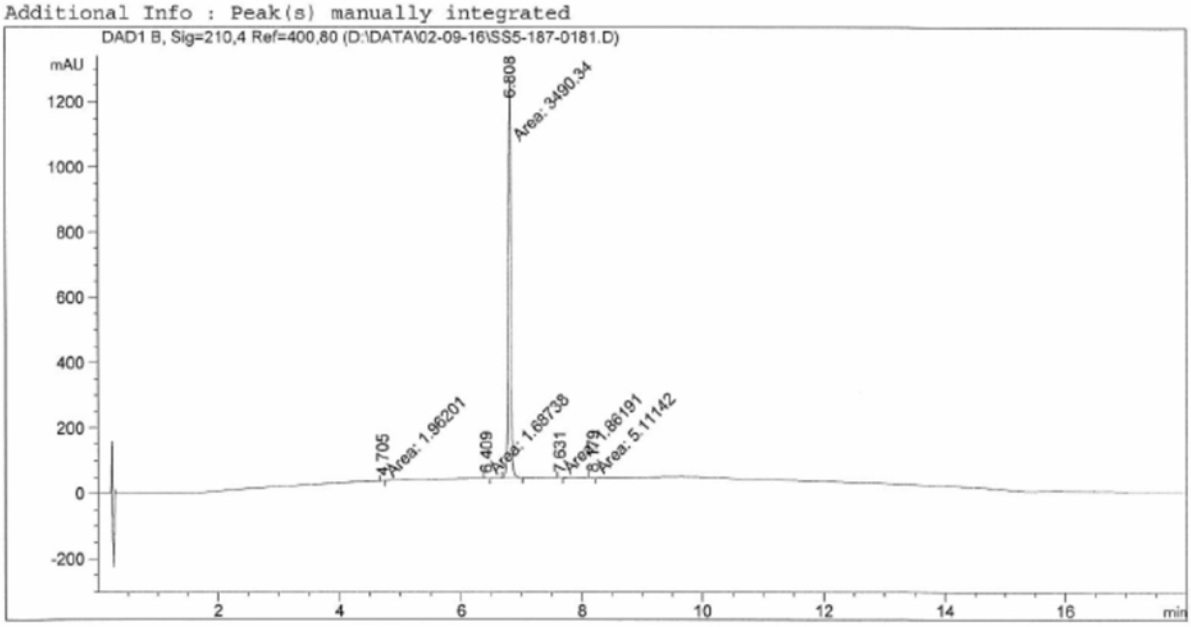


```
=====================================================================
                        Area Percent Report
=====================================================================

Sorted By             :      Signal
Multiplier            :      1.0000
Dilution              :      1.0000
Do not use Multiplier & Dilution Factor with ISTDs


Signal 1: DAD1 B, Sig=210,4 Ref=400,80
```

Peak #	RetTime [min]	Type	Width [min]	Area [mAU*s]	Height [mAU]	Area %
1	4.705	MM	0.0390	1.96201	8.38325e-1	0.0560
2	6.409	MM	0.0537	1.68738	5.24010e-1	0.0482
3	6.808	MM	0.0477	3490.34180	1220.00684	99.6966
4	7.631	MM	0.0494	1.86191	6.27633e-1	0.0532
5	8.179	MM	0.0526	5.11142	1.61934	0.1460
Totals :				3500.96452	1223.61615	

Figure S4. HPLC analysis for purity of EC5026.

```
Acq. Operator    : Agilent                          Seq. Line :   3
Acq. Instrument  : Instrument 1                      Location : Vial 93
Injection Date   : 2/9/2016 4:25:59 PM                  Inj :   1
                                                   Inj Volume : 5.0 µl

Method           : C:\CHEM32\1\METHODS\OD05ET.M
Last changed     : 3/19/2013 7:55:21 AM by Adesis
Method Info      : Column: Chiralpak OD 25cm x 4.6mm, 10um
                   Isocratic method: 95%Hexane + 5%EtOH for 40min
                   Flow: 0.750mL/min
                   Temp: 35°C

Additional Info : Peak(s) manually integrated
```

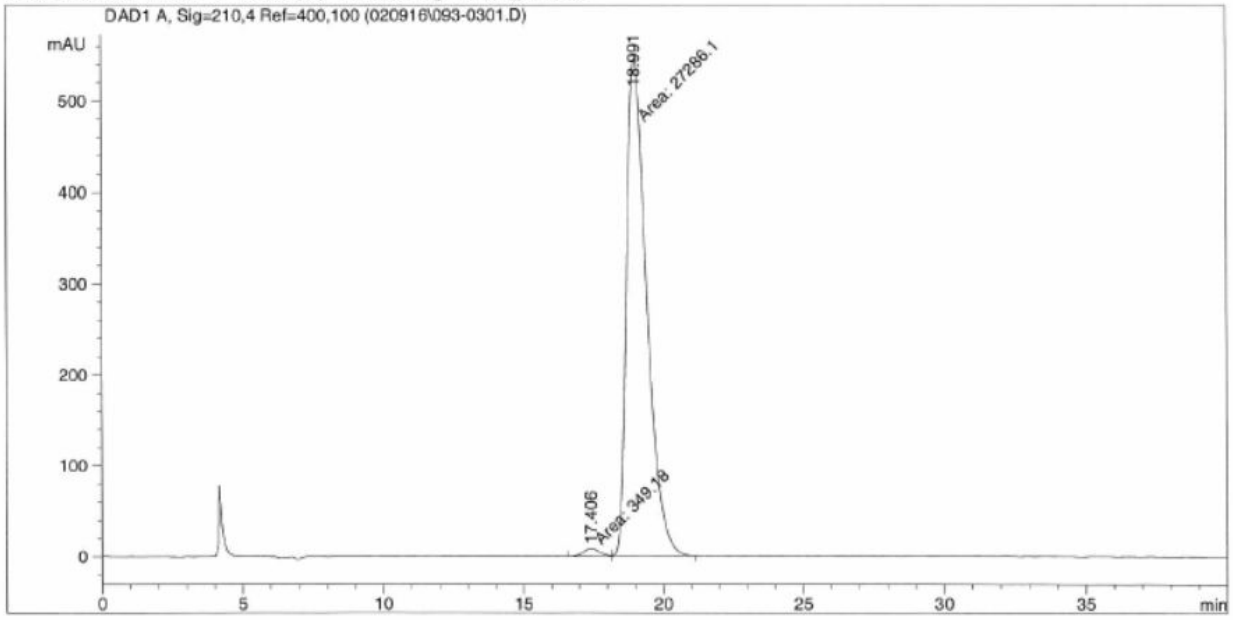


```
=====================================================================
                        Area Percent Report
=====================================================================

Sorted By             :      Signal
Multiplier:                   :      1.0000
Dilution:                     :      1.0000
Use Multiplier & Dilution Factor with ISTDs


Signal 1: DAD1 A, Sig=210,4 Ref=400,100

Peak RetTime Type  Width     Area      Height     Area
  #   [min]        [min]    [mAU*s]    [mAU]       %
----|-------|----|-------|----------|----------|--------|
   1  17.406 MF    0.6841  349.18015    8.50676   1.2635
   2  18.991 FM    0.8337 2.72861e4   545.51416  98.7365

Totals :                  2.76353e4   554.02092
```

Figure S5. HPLC analysis for enantioselectivity of EC5026.

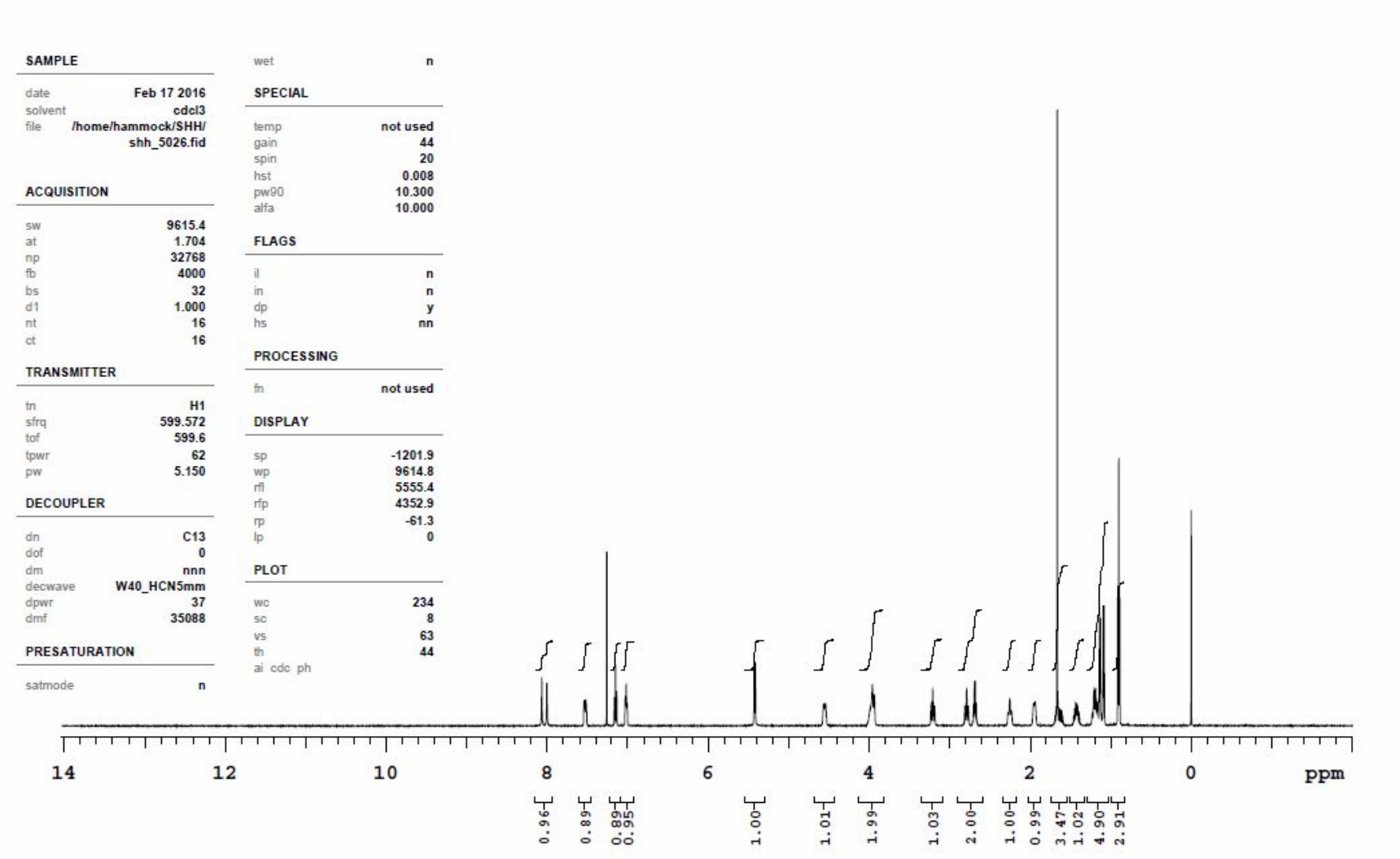

Figure S6. ^{1}H NMR of EC5026

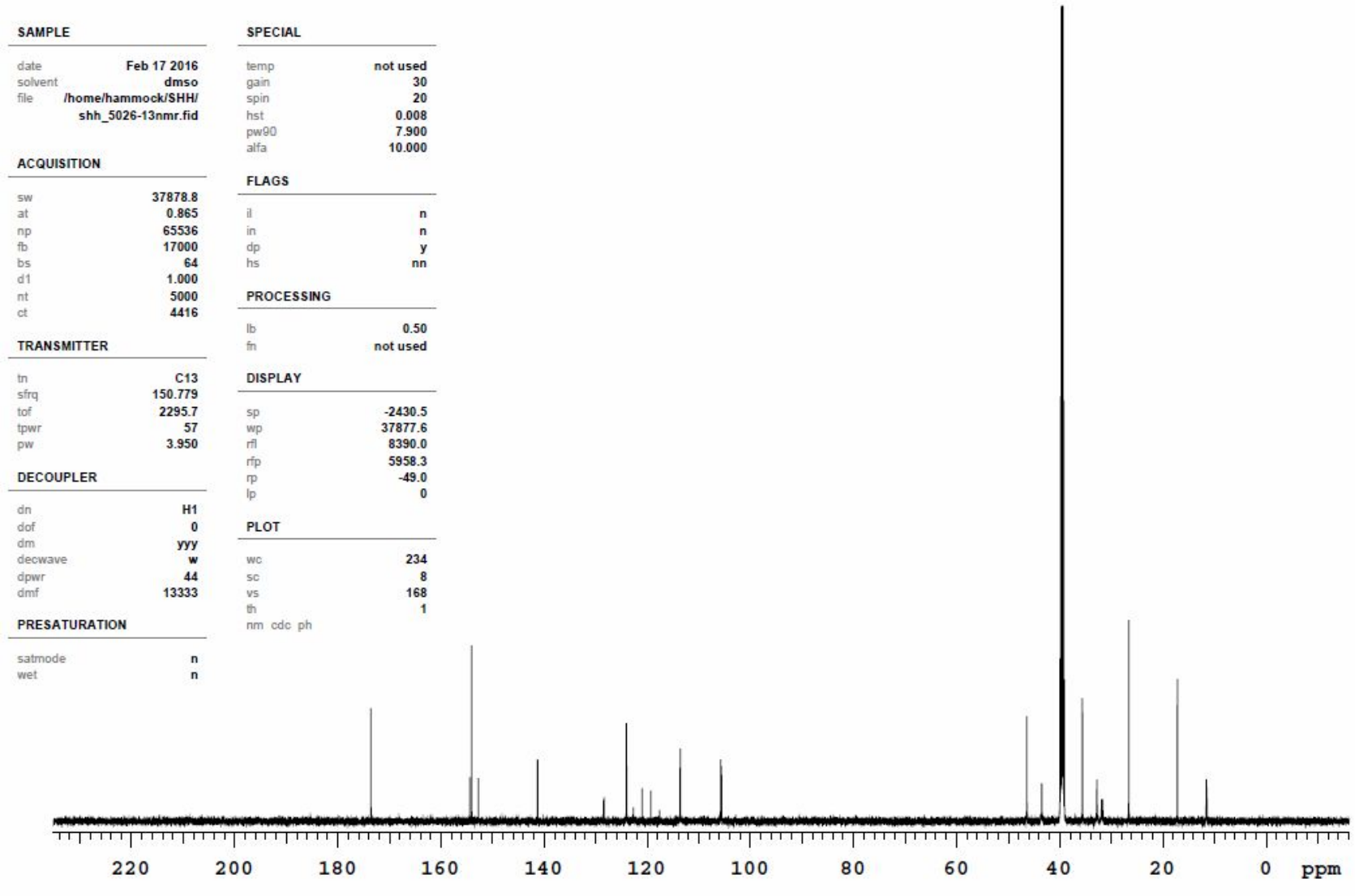

Figure S7. ^{13}C NMR of EC5026

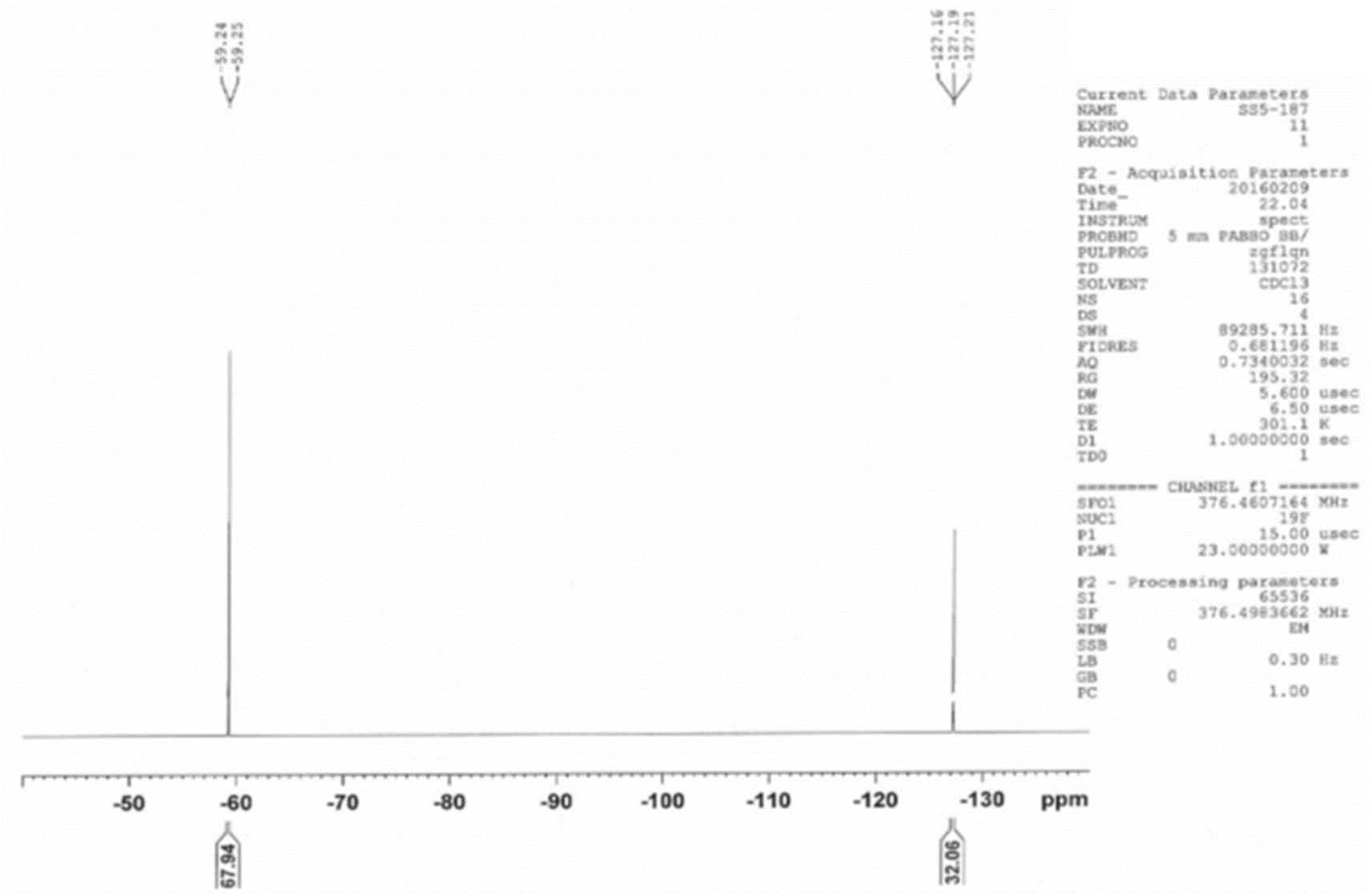

Figure S8. ^{19}F NMR of EC5026

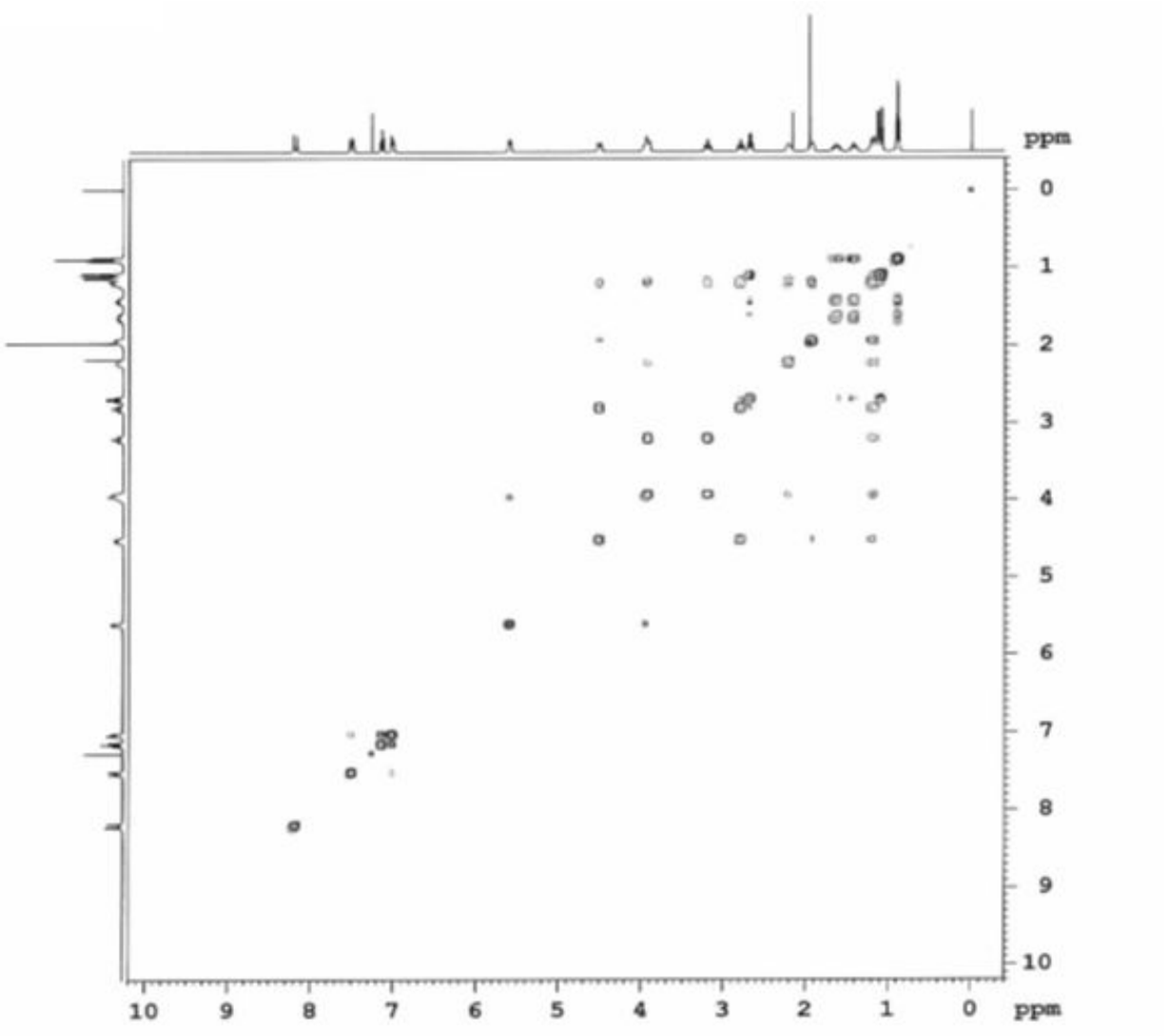

Figure S9. ^{1}H-^{1}H 2D NMR of EC5026

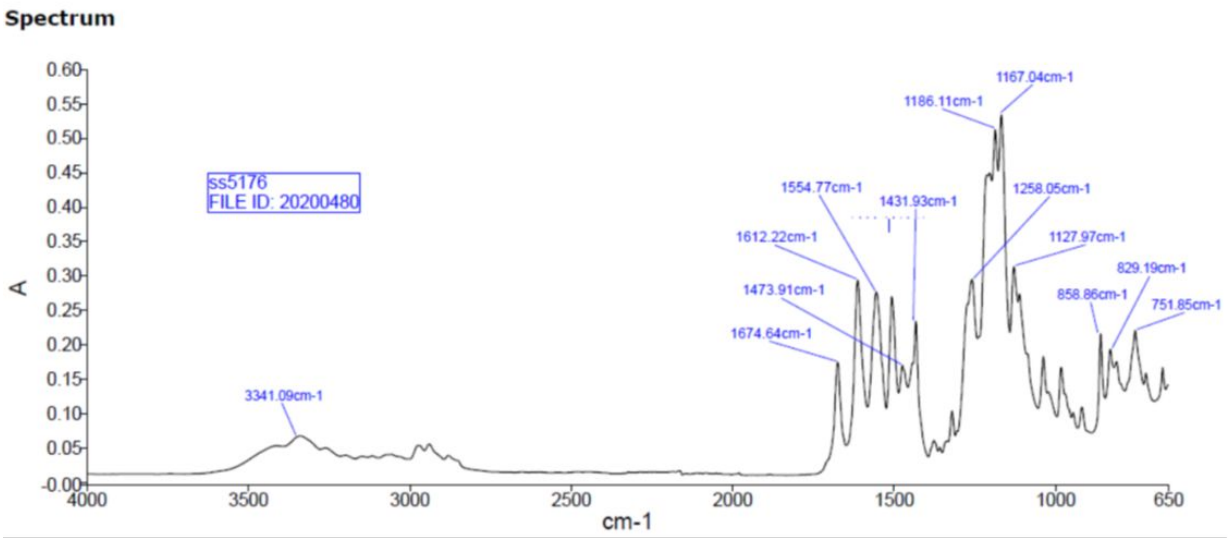

Peak Table

Peak Number	X (cm-1)	Y (A)
1	3341.09	0.07
2	1674.64	0.17
3	1612.22	0.29
4	1554.77	0.28
5	1506.78	0.27
6	1473.91	0.17
7	1431.93	0.23
8	1319.75	0.10
9	1258.05	0.30
10	1186.11	0.51
11	1167.04	0.54
12	1127.97	0.31
13	1036.94	0.18
14	981.65	0.17
15	916.96	0.11
16	858.86	0.22
17	829.19	0.19
18	751.85	0.22
19	666.92	0.17

Figure S10. ATR-FT IR spectrum of EC5026

Table S6. Potential Indications for the use of sEHIs.

Indication	Keywords	Strength of Evidence*	Key References
Painful diabetic neuropathy	Chronic pain, neuropathic pain, ER stress	+++	ref. #8
Osteoarthritis	Chronic pain, inflammatory pain, neuropathic pain	++	ref. #9
Alzheimer's Disease	Neuroinflammation	+++	ref. #10
Parkinson's	Neurodegeneration, neuroinflammation	++	ref. #11
Stroke	Neuroinflammation, ischemia	+++	ref. #12
Cancer	Metastasis, cytokine storm, ER stress, oxidative stress	+++	ref. #13
Diabetes, obesity	Chronic inflammation, metabolic disease	+++	ref. #14
Diabetic retinopathy	Microvascular disease, metabolic disease, oxidative stress	++	ref. #15
NASH/ NAFLD	Metabolic disease, inflammation, hepatic steatosis	++	ref. #16
Myocardial infarction	Ischemia, inflammation	++	ref. #17
Rheumatoid arthritis	Autoimmune, inflammation	+	ref. #18
Hypertension	Chronic inflammation, endothelial dysfunction	+++	ref. #19
Cardiac arrythmia, heart failure	Fibrosis, ischemia, inflammation, cardiac remodeling	+++	ref. #20
Epilepsy	Neuroinflammation	++	ref. #21
Traumatic brain injury	Neuroinflammation	+	ref. #22
Depression	Neuroinflammation, chronic stress	++	ref. #23
Schizophrenia	Neuroinflammation	++	ref. #24
Lupus	Autoimmune	+	ref. #25
COPD	Chronic inflammation	+++	ref. #26
IBD	Chronic inflammation	++	ref. #27
Sepsis/ ARDS	Cytokine storm	++	ref. #28
Asthma	Bronchodilation, inflammation	++	ref. #29
Chronic kidney disease	Fibrosis, vascular disease	++	ref. #30

*determined based on extent of published literature, and depth of published observations (in vitro data, in vivo models, patient correlations, genetic models)

Table S7. List of dual inhibitors/modulators that inhibit sEH as one of target enzymes.

Target	Agent	Disease	Major outcomes
sEH/COX-2	PTUPB	Inflammatory Pain	reduction of inflammatory pain in rats[31]
		Kidney Disease	attenuation of renal damage and inflammation in ZDF Rats[32]
		Cancer	suppression of primary tumor growth and metastasis in mice[33]
			suppression of glioblastoma growth in mice[34]
			potentiation of the antitumor efficacy of cisplatin in mice[35]
			suppression of chemotherapy-induced cytokine/lipid mediator surge and ovarian cancer in mice[36]
			decrease of fibrotic markers in liver injury in mice[37]
		Parkinson's disease	Prevented the reduction of dopamine and its metabolites in Drosophila[38]
		Airway inflammation	Significant inhibition of the development of structural changes in the allergic airways in mice[39]
		Pulmonary fibrosis	Alleviation of the pathological changes in lung tissue and collagen deposition and reduction senescence marker molecules in the lungs in mice[40]
		Non-alcoholic fatty liver disease, sepsis, and acute lung injury	Attenuation of hepatic steatosis, sepsis, and acute lung injury by inhibiting NLRP3 inflammasome activation in mice[41]
sEH/FLAP	diflapolin	Peritonitis	blocked leukotriene formation and suppressed neutrophil infiltration in mice[42]
sEH/5-LOX		Inflammatory Edema	Significant inhibition of the edema in rats[43]
	KM55	inflammation	Significantly inhibition of the LPS-induced adhesion of leukocytes to endothelial cells[44]
sEH/PPAR	RB394	Diabetic complications	Reduction of blood pressure, glucose level, dyslipidemia, hypercholesteremia, and liver/kidney fibrosis in rats[45]
		Inflammatory Edema	anti-inflammatory properties in the zymosan-induced murine paw edema model[46]
sEH/PDE4	*MTTA*	Inflammatory pain	Reduction of inflammatory pain in rats[47]
sEH/FXR	*FXR/sEH dual modulator*	Inflammation	Robustly repressed NF-κB in hepatocarcinoma cells and reduced the Pam3CSK4 stimulated release of TNFα from the T-cell line HuT-78[48]
		Metabolic liver disorders	Prevention of hepatic steatosis and fibrosis in mice[49]
sEH/FAAH	*FAAH/sEH dual inhibitor*	Inflammatory pain	improved cross-species potencies against both FAAH and sEH[50]
sEH/C-RAF	*t*-CUPM	Pancreatic carcinoma	Inhibition of murine pancreatic carcinoma growth[51]

References

1. Lee, K.S.; Liu, J.Y.; Wagner, K.M.; Pakhomova, S.; Dong, H.; Morisseau, C.; Fu, S.H.; Yang, J.; Wang, P.; Ulu, A.; Mate, C.A.; Nguyen, L.V; Hwang, S.H.; Edin, M.L.; Mara, A.A.; Wulff, H.; Newcomer, M.E.; Zeldin, D.C.; Hammock, B.D. Optimized inhibitors of soluble epoxide hydrolase improve in vitro target residence time and in vivo efficacy. *J. Med. Chem*. **2014**, *57(16)*, 7016-7030.

2. Lee, K.S.S.; Morisseau, C.; Yang, J.; Wang, P.; Hwang, S.H.; Hammock, B.D. Forster resonance energy transfer competitive displacement assay for human soluble epoxide hydrolase. *Anal. Chem*. **2013**, *434(2)*, 259-268.

3. Roehrl, M.H.A.; Kang, S.H.; Aramburu, J.; Wagner, G.; Rao, A.; Hogan, P.G. Selective inhibition of calcineurin-nfat signaling by blocking protein-protein interaction with small organic molecules. *Proc. Natl. Acad. Sci. USA* **2004**, *101(20)*, 7554-7559.

4. Wang, Z.X. An exact mathematical expression for describing competitive-binding of 2 different ligands to a protein molecule. *Febs Lett*. **1995**, *360(2)*, 111-114.

5. Hidalgo, J.; Raub, T. J.; Borchardt, R. T. Characterization of the human colon carcinoma cell line (Caco-2) as a model system for intestinal epithelial permeability. *Gastroenterology* **1989**, *96*, 736-749.

6. Madan, A.; Graham, R.A.; Carroll, K.M.; Mudra, D.R.; Burton, L.A.; Krueger, L.A.; Downey, A.D.; Czerwinski, M.; Forster, J.; Ribadeneira, M.D.; Gan, L.S.; LeCluyse, E.L.; Zech, K.; Robertson, P, Jr..; Koch, P.; Antonian, L.; Wagner, G.; Yu, L.; Parkinson, A. Effects of prototypical microsomal enzyme inducers on cytochrome P450 expression in cultured human hepatocytes. *Drug Metab. Dispos*. **2003**, *31(4)*, 421-431.

7. Otten, J.N.; Hingorani, G.P.; Hartley, D.P.; Kragerud, S.D.; Franklin, R.B. An in vitro, high throughput, seven CYP cocktail inhibition assay for the evaluation of new chemical entities using LC-MS/MS. *Drug Metab. Lett*. **2011**, *5(1)*, 17-24.

8. Wagner, K.; Yang, J.; Inceoglu, B.; Hammock, B.D. Soluble epoxide hydrolase inhibition is antinociceptive in a mouse model of diabetic neuropathy. *J. Pain* **2014**, *15(9)*, 907-914.

9. McReynolds, C.B.; **Hwang, S.H.**; Yang, J.; Wan, D.; Wagner, K.; Morisseau, C.; Li, D.; Schmidt, W.K.; Hammock, B.D. Pharmaceutical Effects of Inhibiting the Soluble Epoxide Hydrolase in Canine Osteoarthritis. *Front. Pharmacol*. **2019**, *10*, 533.

10. Griñán-Ferré, C.; Codony, S.; Pujol, E.; Yang, J.; Leiva, R.; Escolano, C.; Puigoriol-Illamola, D.; Companys-Alemany, J.; Corpas, R.; Sanfeliu, C.; Pérez, B.; Loza, M.I.; Brea, J.; Morisseau, C.; Hammock, B.D.; Vázquez, S.; Pallàs, M.; Galdeano, C. Pharmacological Inhibition of Soluble Epoxide Hydrolase as a New Therapy for Alzheimer's Disease. *Neurotherapeutics* **2020** Jun 2. [Online ahead of print]. DOI: 10.1007/s13311-020-00854-1. Published Online: June 2, 2020. https://link.springer.com/article/10.1007%2Fs13311-020-00854-1 (accessed Sept 14, 2020).

11. Ren, Q.; Ma, M.; Yang, J.; Nonaka, R.; Yamaguchi, A.; Ishikawa, K.I.; Kobayashi, K.; Murayama, S.; Hwang, S.H.; Saiki, S.; Akamatsu, W.; Hattori, N.; Hammock, B.D.; Hashimoto, K. Soluble epoxide hydrolase plays a key role in the pathogenesis of Parkinson's disease. *Proc. Natl. Acad. Sci. USA* **2018**, *115*, E5815-E5823.

12. Dorrance, A.M.; Rupp, N.; Pollock, D.M.; Newman, J.W.; Hammock, B.D.; Imig, J.D. An epoxide hydrolase inhibitor, 12-(3-adamantan-1-yl-ureido)dodecanoic acid (AUDA), reduces ischemic cerebral infarct size in stroke-prone spontaneously hypertensive rats. *J. Cardiovasc. Pharmacol*. **2005**, *46(6)*, 842–848.

13. Zhang, G.; Panigrahy, D.; Hwang, S.H.; Yang, J.; Mahakian, L.M.; Wettersten, H.I.; Liu, J.-Y.; Wang, Y.; Ingham, E.S.; Tam, S.; Kieran, M.W.; Weiss, R.H.; Ferrara, K.W.; Hammock, B.D. Dual inhibition of cyclooxygenase-2 and soluble epoxide hydrolase synergistically suppresses primary tumor growth and metastasis. *Proc. Natl. Acad. Sci. USA* **2014**, *111,* 11127-11132.

14. Luria, A.; Bettaieb, A.; Xi, Y.; Shieh, G.; Liu, H.; Inoue, H.; Tsai, H.; Imig, J.D.; Haj, F.G.; Hammock, B.D. Soluble epoxide hydrolase deficiency alters pancreatic islet size and improves glucose homeostasis in a model of insulin resistance. *Proc. Natl. Acad. Sci. U.S.A*. **2011**, *108(22)*, 9038–9043.

15. Hu, J.; Dziumbla, S.; Lin, J.; Bibli, S.; Zukunft, S.; de Mos, J.; Awwad, K.; Frömel, T.; Jungmann, A.; Devraj, K.; Cheng, Z.; Wang, L.; Fauser, S.; Eberhart, C.G.; Sodhi, A.; Hammock, B.D.; Liebner, S.; Müller, O.J.; Glaubitz, C.; Hammes, H.; Popp, R.; Fleming, I. Inhibition of soluble epoxide hydrolase prevents diabetic retinopathy. *Nature* **2017**, *552 (7684)*, 248-252.

16. Liu, Y.; Dang, H.; Li, D.; Pang, W.; Hammock, B.D.; Zhu, Y. Inhibition of soluble epoxide hydrolase attenuates high-fat-diet-induced hepatic steatosis by reduced systemic inflammatory status in mice. *PLoS ONE* **2012**, *7 (6)*, e39165.

17. Islam, O.; Patil, P.; Goswami, S.K.; Razdan, R.; Inamdar, M. N.; Rizwan, M.; Mathew, J.; Inceoglu, B.; Stephen Lee, K.S.; Hwang, S.H.; Hammock, B.D. Inhibitors of soluble epoxide hydrolase minimize ischemia-reperfusion-induced cardiac damage in normal, hypertensive, and diabetic rats. *Cardiovasc. Ther*. **2017**, *35*, e12259.

18. Teixeira, J.M.; Abdalla, H.B.; Basting, R.T.; Hammock, B.D.; Napimoga, M.H.; Clemente-Napimoga, J.T. Peripheral soluble epoxide hydrolase inhibition reduces hypernociception and inflammation in albumin-induced arthritis in temporomandibular joint of rats. *Int. Immunopharmacol*. **2020**, *87*, 106841.

19. Imig, J.D.; Zhao, X.; Capdevila, J.H.; Morisseau, C.; Hammock, B.D. Soluble epoxide hydrolase inhibition lowers arterial blood pressure in angiotensin II hypertension. *Hypertension* **2002**, *39*, 690–694

20. Monti, J.; Fischer, J.; Paskas, S.; Heinig, M.; Schulz, H.; Gösele, C.; Heuser, A.; Fischer, R.; Schmidt, C.; Schirdewan, A.; Gross, V.; Hummel, O.; Maatz, H.; Patone, G.; Saar, K.; Vingron, M.; Weldon, S.M.; Lindpaintner, K.; Hammock, B.D.; Rohde, K.; Dietz, R.; Cook,

S.A.; Schunck, W.; Luft, F.C.; Hubner, N. Soluble epoxide hydrolase is a susceptibility factor for heart failure in a rat model of human disease. *Nat. Genet*. **2008**, *40(5)*, 529–537

21. Shen, Y.; Peng, W.; Chen, Q.; Hammock, B.D.; Liu, J.; Li, D.; Yang, J.; Ding, J.; Wang, X. Anti-inflammatory treatment with a soluble epoxide hydrolase inhibitor attenuates seizures and epilepsy-associated depression in the LiCl-pilocarpine post-status epilepticus rat model. *Brain Behav. Immun*. **2019**, *81*, 535-544.

22. Hung, T.-H.; Shyue, S.-K.; Wu, C.-H.; Chen, C.-C.; Lin, C.-C.; Chang, C.-F.; Chen, S.-F. Deletion or inhibition of soluble epoxide hydrolase protects against brain damage and reduces microglia-mediated neuroinflammation in traumatic brain injury. *Oncotarget* **2017**, *8 (61)*, 103236-103260.

23. Ren, Q.; Ma, M.; Ishima, T.; Morisseau, C.; Yang, J.; Wagner, K.M.; Zhang, J.; Yang, C.; Yao, W.; Dong, C.; Han, M.; Hammock, B.D.; Hashimoto, K. Gene deficiency and pharmacological inhibition of soluble epoxide hydrolase confers resilience to repeated social defeat stress. *Proc. Natl. Acad. Sci. USA* **2016**, *113 (13)*, E1944-E1952.

24. Ma, M.; Ren, Q.; Fujita, Y.; Ishima, T.; Zhang, J.; Hashimoto, K. Effects of AS2586114, a soluble epoxide hydrolase inhibitor, on hyperlocomotion and prepulse inhibition deficits in mice after administration of phencyclidine. *Pharmacol. Biochem. Behav*. **2013**, *110*, 98-103.

25. Klocke, J.; Ulu, A.; Wu, K.; Rudolph, B.; Dragun, D.; Gollasch, M.; Schunck, W.-H.; Hammock, B.D.; Riemekasten, G.; Enghard, P. Prophylactic inhibition of soluble epoxide hydrolase delays onset of nephritis and ameliorates kidney damage in NZB/W F1 mice. *Sci. Rep.* **2019**, *9 (1)*, 8993.

26. Wang, L.; Yang, J.; Guo, L.; Uyeminami, D.; Dong, H.; Hammock, B.D.; Pinkerton, K.E. Use of a soluble epoxide hydrolase inhibitor in smoke-induced chronic obstructive pulmonary disease. *Am. J. Respir. Cell Mol. Biol.* **2012**, *46 (5)*, 614-622.

27. Zhang, W.; Yang, A.L.; Liao, J.; Li, H.; Dong, H.; Chung, Y.T.; Bai, H.; Matkowskyj, K.A.; Hammock, B.D.; Yang, G. Soluble epoxide hydrolase gene deficiency or inhibition attenuates chronic active inflammatory bowel disease in IL-10(-/-) mice. *Dig. Dis. Sci*. **2012**, *57(10)*, 2580–2591.

28. Chen, Z.; Tang, Y.; Yu, J.; Dong, R.; Yang, Y.; Fu, M.; Luo, J.; Hu, S.; Wang, D.W.; Tu, L.; Xu, X. sEH Inhibitor Tppu Ameliorates Cecal Ligation and Puncture-Induced Sepsis by Regulating Macrophage Functions. *Shock* **2020**, *53 (6)*, 761–771.

29. Yang, J.; Bratt, J.; Franzi, L.; Liu, J.; Zhang, G.; Zeki, A.A.; Vogel, C.F.; Williams, K.; Dong, H.; Lin, Y.; Hwang, S.H.; Kenyon, N.J.; Hammock, B.D. Soluble Epoxide Hydrolase Inhibitor Attenuates Inflammation and Airway Hyperresponsiveness in Mice. *Am. J. Respir. Cell Biol*. **2015**, *52*, 46-55.

30. Vacková, Š.; Kopkan, L.; Kikerlová, S.; Husková, Z.; Sadowski, J.; Kompanowska-Jezierska, E.; Hammock, B.D.; Imig, J.D.; Táborský, M.; Melenovský, V.; Červenka, L. Pharmacological Blockade of Soluble Epoxide Hydrolase Attenuates the Progression of Congestive Heart

Failure Combined With Chronic Kidney Disease: Insights From Studies With Fawn-Hooded Hypertensive Rats. *Front Pharmacol.* **2019**, *10*,18.

31. Hwang, S.H., et al., Synthesis and structure-activity relationship studies of urea-containing pyrazoles as dual inhibitors of cyclooxygenase-2 and soluble epoxide hydrolase. *J Med Chem*, **2011**. *54*(8), 3037-3050

32. Hye Khan, M.A., et al., A dual COX-2/sEH inhibitor improves the metabolic profile and reduces kidney injury in Zucker diabetic fatty rat. *Prostaglandins Other Lipid Mediat*, **2016**. *125,* 40-47

33. Zhang, G., et al., Dual inhibition of cyclooxygenase-2 and soluble epoxide hydrolase synergistically suppresses primary tumor growth and metastasis. *Proc Natl Acad Sci USA*, **2014**. *111*(30), 11127-11132

34. Li, J., et al., COX-2/sEH dual inhibitor PTUPB suppresses glioblastoma growth by targeting epidermal growth factor receptor and hyaluronan mediated motility receptor. *Oncotarget*, **2017**. *8*(50), 87353-87363

35. Wang, F., et al., COX-2/sEH Dual Inhibitor PTUPB Potentiates the Antitumor Efficacy of Cisplatin. *Mol Cancer Ther*, **2018**. *17*(2), 474-483

36. Gartung, A.; Yang, J.; Sukhatme, V.P.; Bielenberg, D.R.; Fernandes, D.; Chang, J., Schmidt, B.A.; Hwang, S.H.; Zurakowski, D.; Huang, S.; Kieran, M.W.; Hammock, B.D., Panigrahy, D. Suppression of chemotherapy-induced cytokine/lipid mediator surge and ovarian cancer by a dual COX-2/sEH inhibitor. *Proc. Natl. Acad. Sci. USA* **2019**, *116*, 1698-1703

37. Harris, T.R., et al., Celecoxib does not protect against fibrosis and inflammation in a carbon tetrachloride-induced model of liver injury. *Mol Pharmacol*, **2018**. *94*(2), 834-841

38. Lakkappa, N.; Krishnamurthy, P.T.; Yamjala, K.; **Hwang, S.H.**; Hammock, B.D.; Babu, B. Evaluation of antiparkinson activity of PTUPB by measuring dopamine and its metabolites in Drosophila melanogaster: LC-MS/MS method development. *J. Pharmaceut. Biomed*. **2018**, *149*, 457-464

39. Dileepan, M.; Rastle-Simpson S.; Greenberg Y.; Wijesinghe D.S.; Kumar N.G.; Yang J.; Hwang S.H.; Hammock B.D.; Sriramarao P.; Rao S.P. Effect of Dual sEH/COX-2 Inhibition on Allergen-Induced Airway Inflammation. *Front Pharmacol*. **2019**, *10*, 1118

40. Zhang, C.Y.; Duan, JX.; Yang, H.H.; Sun, C.C.; Zhong, W.J.; Tao, J.H.; Guan, X.X.; Jiang, H.L.; Hammock, B.D.; Hwang, S.H.; Zhou, Y.; Guan, C.X. COX-2/sEH dual inhibitor PTUPB alleviates bleomycin-induced pulmonary fibrosis in mice via inhibiting senescence. *FEBS J*. **2020**, *287*, 1666-1680

41. (a) Sun, C.C.; Zhang, C.Y.; Duan, J.X.; Guan, X.X.; Yang, H.H.; Jiang, H.L.; Hammock, B.D.; Hwang, S.H.; Zhou, Y.; Guan, C.X.; Liu, S.K.; Zhang, J. PTUPB ameliorates high-fat diet-induced non-alcoholic fatty liver disease via inhibiting NLRP3 inflammasome activation in mice. *Biochem. Biophys. Res. Commun*. **2020**, *523*, 1020-1026. (b) Zhang, Y.F.; Sun, C.C.; Duan, J.X.; Yang, H.H.; Zhang, C.Y.; Xiong, J.B.; Zhong, W.J.; Zu, C.; Guan, X.X.; Jiang, H.L.; Hammock, B.D.; Hwang, S.H.; Zhou, Y.; Guan, C.X. A COX-2/sEH dual inhibitor

PTUPB ameliorates cecal ligation and puncture-induced sepsis in mice via anti-inflammation and anti-oxidative stress. *Biomed Pharmacother*. **2020**, *126*,109907. (C) Yang, H.H.; Duan, J.X.; Liu, S.K.; Xiong, J.B.; Guan, X.X.; Zhong, W.J.; Sun, C.C.; Zhang, C.Y.; Luo, X.Q.; Zhang, Y.F.; Chen, P.; Hammock, B.D.; Hwang, S.H.; Jiang, J.X.; Zhou, Y.; Guan, C.X. A COX-2/sEH dual inhibitor PTUPB alleviates lipopolysaccharide-induced acute lung injury in mice by inhibiting NLRP3 inflammasome activation. *Theranostics* **2020**, *10*, 4749-4761.

42. (a)Garscha, U., et al., Pharmacological profile and efficiency in vivo of diflapolin, the first dual inhibitor of 5-lipoxygenase-activating protein and soluble epoxide hydrolase. *Sci Rep-UK*, **2017**. *7*(1): p. 9398. (b) Vieider L, Romp E, Temml V, Fischer J, Kretzer C, Schoenthaler M, Taha A, Hernández-Olmos V, Sturm S, Schuster D, Werz O, Garscha U, Matuszczak B. *ACS Med Chem Lett*. **2018**, *10(1),* 62-66.

43. Nandha, B., S.A. Ramareddy, and H. Kuntal, Synthesis of substituted fluorobenzimidazoles as inhibitors of 5-lipoxygenase and soluble epoxide hydrolase for anti-inflammatory activity. *Arch Pharm Chem Life Sci*, **2018**. *351,* e1800030

44. Meirer, K., et al., Synthesis and structure-activity relationship studies of novel dual inhibitors of soluble epoxide hydrolase and 5-lipoxygenase. *J Med Chem*, **2013**. *56*(4): p. 1777–1781

45. Hye Khan, M.A., Kolb, L., Skibba, M., Hartmann, M., Blöcher, R., Proschak, E., Imig, J.D., A novel dual PPARγ agonist/sEH inhibitor treats diabetic complications in a rat model of type 2, *Diabetologia*. **2018**, DOI: 10.1007/s00125-018-4685-0

46. Schierle, S., et al., Boosting Anti-Inflammatory Potency of Zafirlukast by Designed Polypharmacology. *J Med Chem*, **2018**. *61*(13): p. 5758-5764

47. Blöcher, R.; Wagner, K.M.; Gopireddy, R.R.; Harris, T.R.; Wu, H.; Barnych, B.; Hwang, S.H.; Xiang, Y.K.; Proschak, E.; Morisseau, C.; Hammock, B.D. Orally Available Soluble Epoxide Hydrolase/Phosphodiesterase 4 Dual Inhibitor Treats Inflammatory Pain. *J. Med. Chem*. **2018**, *61*, 3541-3550

48. Schmidt, J., et al., A Dual Modulator of Farnesoid X Receptor and Soluble Epoxide Hydrolase To Counter Nonalcoholic Steatohepatitis. *J Med Chem*, **2017**. *60*(18): p. 7703-7724.

49. Hye Khan MA, Schmidt J, Stavniichuk A, Imig JD, Merk D. Biochem Pharmacol. 2019, 166, 212-221. (b) Schierle S, Helmstädter M, Schmidt J, Hartmann M, Horz M, Kaiser A, Weizel L, Heitel P, Proschak A, Hernandez-Olmos V, Proschak E, Merk D. *ChemMedChem*. **2020**, *15(1)*, 50-67

50. Kodani, S.D.; Wan, D.; Wagner, K.M.; Hwang, S.H.; Morisseau, C.; Hammock, B.D. Design and Potency of Dual Soluble Epoxide Hydrolase/Fatty Acid Amide Hydrolase Inhibitors. *ACS Omega* **2018**, *3*, 14076-14086

51. (a)Liao, J.; Hwang, S.H.; Li, H.; Liu, J.Y.; Hammock, B.D.; Yang, G.Y. Inhibition of Chronic Pancreatitis and Murine Pancreatic Intraepithelial Neoplasia by a Dual Inhibitor of c-RAF and Soluble Epoxide Hydrolase in LSL-KrasG^{12}D/Pdx-1-Cre Mice. *Anticancer Res.* **2016**, *36*, 27-37. (b)Liao, J.; Hwang, S.H.; Li, H.; Yang, Y.; Yang, J.; Wecksler, A.T.; Liu, J.Y.; Hammock, B.D.; Yang, G.Y. Inhibition of mutant KrasG12D-initiated murine pancreatic carcinoma

growth by a dual c-Raf and soluble epoxide hydrolase inhibitor *t*-CUPM. *Cancer Lett.* **2016**, *371*, 187-193.